Journal of Hydrology 538 (2016) 743–753

Contents lists available at ScienceDirect

Journal of Hydrology

journal homepage: www.elsevier.com/locate/jhydrol

Using heat as a tracer to estimate the depth of rapid porewater advection below the sediment–water interface

Alicia M. Wilson [a,b,*], Gwendolyn L. Woodward [b], William B. Savidge [c]

[a] Dept. Earth & Ocean Sciences, University of South Carolina, Columbia, SC 29208, United States
[b] Environment & Sustainability Program, University of South Carolina, United States
[c] Skidaway Institute of Oceanography, University of Georgia, Savannah, GA 31411, United States

ARTICLE INFO

Article history:
Received 2 October 2015
Received in revised form 25 February 2016
Accepted 24 April 2016
Available online 30 April 2016
This manuscript was handled by Peter K. Kitanidis, Editor-in-Chief, with the assistance of Hund-Der Yeh, Associate Editor

Keywords:
Hyporheic flow
Benthic exchange
Heat
Inverse model
Submarine groundwater discharge

SUMMARY

Rapid exchange of surface waters and porewaters in shallow sediments has important biogeochemical implications for streams and marine systems alike, but mapping these important reaction zones has been difficult. As a means of bridging the gap between the stream and submarine groundwater discharge communities we suggest that the rapid, transient mixing in this zone be called "hydrodynamic exchange". We then present a new model, MATTSI, which was developed to estimate the timing, depth and magnitude of hydrodynamic exchange below the sediment–water interface by inverting thermal time-series observations. The model uses an effective thermal dispersion term to emulate 3-D hydrodynamic exchange in a 1-D model. The effective dispersion is assumed to decline exponentially below the sediment water interface. Application of the model to a synthetic dataset and two field datasets from 50 km offshore in the South Atlantic Bight shows that exchange events can be clearly identified from thermal data. The model is relatively insensitive to realistic errors in sensor depth and thermal conductivity. Although the datasets tested here were too shallow to fully span the depth of flushing, we were able to estimate the depth of hydrodynamic exchange via sensitivity studies.

1. Introduction

The geochemical composition of surface water is influenced by discharging groundwater and by circulation of surface waters through underlying sediments (Boano et al., 2014; Brunke and Gonser, 1997; Burnett et al., 2003; Moore, 2010; 1999; Santos et al., 2012; Sophocleous, 2002). This exchange affects streams and the ocean in parallel ways, and mapping subsurface mixing zones has become a high priority in freshwater and marine systems alike. The primary purpose of this paper is to present a new method to determine the depth of rapid, transient flushing below the sediment–water interface in stream and marine settings. Before introducing this method in detail, however, it will be helpful to establish some common terminology.

The hydrologic and marine communities share similar scientific goals with respect to fluid and biogeochemical exchanges across the sediment–water interface, but they do not share terminology (Table 1). Where hydrologists refer to surface water–groundwater interactions, oceanographers refer to submarine groundwater discharge (SGD), a term that emphasizes the export of nutrients, metals, and carbon from sediments to the ocean. As reviewed by Boano et al. (2014), hydrologists studying surface water–groundwater interactions distinguish between groundwater flow and hyporheic flow. The former implies regional flow, whereas the latter refers to relatively small-scale flows of water that originate in the surface water, travel below the sediment–water interface, and return to the surface water. Hyporheic flow is further broken down into hydrostatic (driven by spatial or temporal variations in the water level of the stream) and hydrodynamic components (driven by turbulence, currents, density gradients, or surficial pressure gradients). In contrast, the oceanographic literature uses the term groundwater to refer to fresh and saline porewater, regardless of origin or flow path (Burnett et al., 2003). Fresh and saline SGD are commonly differentiated, but saline SGD encompasses flow processes ranging from meter-scale tidal pumping to processes like geothermal convection (Sanford et al., 1998), which span tens of kilometers. Centimeter-scale flows, for example those driven by high-frequency waves (King et al., 2009) or current-ripple interactions (Huettel et al., 1996), are not always included in the broad definition of SGD (Moore, 2010), but these processes clearly cause water and solutes to migrate across the seafloor in sandy marine settings (Precht et al., 2004; Reimers et al., 2004;

* Corresponding author at: Dept. Earth & Ocean Sciences, University of South Carolina, Columbia, SC 29208, United States.

http://dx.doi.org/10.1016/j.jhydrol.2016.04.047
0022-1694/

Table 1
Terminology.

Hydrology	Oceanography and coastal hydrology	This paper
Groundwater (connotes regional flow of fresh groundwater)	Groundwater (fresh or saline, any flow process)	Groundwater (regional flow of fresh or saline groundwater)
Hyporheic flow	No widely accepted term	Hyporheic and hypokymatic[a] flow
Hydrostatic component	No single term	Hydrostatic component
Hydrodynamic component	Benthic exchange	Hydrodynamic exchange
Discharge from hyporheic and groundwater flow systems	Submarine groundwater discharge (SGD)	Discharge across the sediment–water interface
Stream stage	Sea level, water level	Surface-water level
The subsurface	The sediment column	The subsurface
Subsurface	Sub-seafloor	Subsurface

[a] "Under the tide" or "under the swell".

Santos et al., 2012). These small-scale processes are typically grouped and referred to as benthic exchange.

We propose a hybrid terminology that will allow us to communicate clearly with both communities (Table 1). In this paper, "groundwater" will to refer to fresh and saline porewater that is part of a regional flow system. This means that "groundwater" includes regional flow of saline groundwater below the seafloor, including submarine geothermal convection (Sanford et al., 1998; Wilson, 2005, 2003), compaction-driven flow (Bethke, 1985; Osborne and Swarbrick, 1997; Wilson et al., 1999), and haline convection (Ranganathan and Hanor, 1988; Smith, 2004; Wilson, 2005). As a parallel to hyporheic flow in streams and hypolentic flow in lakes (Aseltyne et al., 2006), we propose the term "hypokymatic flow," meaning "under the tide" or "under the swell," to refer to relatively small-scale flows that originate in the ocean, travel through sediments, and return to the ocean. As emphasized by Boano et al. (2014) for hyporheic flow, the difference between hypokymatic flow and regional groundwater flow depends on the scale of interest. Continuing in parallel with freshwater terminology, the hydrostatic component of hypokymatic flow is driven by tidal fluctuations or other temporal and spatial variations in sea level (e.g. Santos et al., 2010). The hydrodynamic component of hypokymatic flow is benthic exchange. We propose the hybrid "hydrodynamic exchange" as a concise term to describe both benthic exchange in marine systems and the hydrodynamic component of hyporheic flow in streams (Table 1).

This paper focuses on mapping hydrodynamic exchange. As recently reviewed by Boano et al. (2014) for streams and Huettel et al. (2014) for marine systems, hydrodynamic exchange can be a major contributor to biogeochemical cycling. Rapid exchange below the sediment–water interface drives mixing between typically oxygenated surface waters and highly reduced porewaters. This exchange also allows particle transport and filtration (Huettel and Rusch, 2000; Packman et al., 2000) that delivers particle-associated metals, carbon, and phosphorus to the sediments. This zone of hydrodynamic exchange supports rapid microbial metabolism (Boano et al., 2014; Ehrenhauss and Huettel, 2004; Huettel and Rusch, 2000; Jahnke et al., 2005) and hosts such processes as denitrification (Laursen and Seitzinger, 2002; Mulholland et al., 2008; Rao et al., 2007), metals speciation (Harvey and Fuller, 1998; Huettel et al., 1998), remineralization of organic carbon (Conant et al., 2004; Cook et al., 2007; Janssen et al., 2005), and biodegradation of organic contaminants (Conant et al., 2004).

Hydrodynamic exchange can be highly transient. The depth and intensity of hydrodynamic exchange in streams varies with discharge, which can change dramatically on time scales of hours or minutes. In marine settings, hydrodynamic exchange can be affected by bi-directional flow on tidal time scales. Thermal instabilities can also drive flushing below the sediment–water interface (Moore and Wilson, 2005; Rocha, 2000) or enhance exchange where hydraulic gradients provide the primary driver for flow (Boano et al., 2009; Jin et al., 2011). This paper presents a method that inverts thermal time series data to estimate the timing and depth of transient hydrodynamic exchange.

2. Heat as a tracer

Heat has been used as an inexpensive and effective tracer in a wide range of hydrogeologic systems (Anderson, 2005) and has found particular use as a tracer for monitoring groundwater flow and hyporheic exchange below streams (Boano et al., 2014; Constantz, 2008). Heat has found similar use as a tracer for submarine groundwater discharge (SGD) in marine and coastal systems (Befus et al., 2013; Cho et al., 2010; Martin et al., 2006; Moore and Wilson, 2005; Moore et al., 2002; Taniguchi, 2000). Many studies have determined groundwater flow rates using methods based on one-dimensional analytical solutions to the heat transport equation (Bredehoeft and Papadopulos, 1965; Hatch et al., 2006; Stallman, 1963).

$$\frac{\partial T}{\partial t} = \kappa_e \frac{\partial^2 T}{\partial z^2} - \phi v \frac{\rho_f c_f}{C} \frac{\partial T}{\partial z} \tag{1}$$

where ϕ is the porosity, ρ_f is the density of water, c_f is the specific heat capacity of water, κ_e is the effective thermal diffusivity, v is the average linear velocity of the groundwater, z is depth below the sediment–water interface (positive downward), and C is the average heat capacity of the saturated sediment.

$$C = \phi \rho_f c_f + (1-\phi)\rho_s c_s \tag{2}$$

where ρ_s is the density of the solid grains and c_s is the specific heat capacity of the solid grains.

Recently Bhaskar et al. (2012) demonstrated that thermal records can be used to analyze co-occurring hyporheic and groundwater flow. Their approach built on bench-scale tracer studies (Elliott and Brooks, 1997; Elliott et al., 1997) that indicated that shallow 3-D hydrodynamic exchange could be accommodated in a 1-D framework by modifying the effective thermal diffusivity to include an effective dispersion term. If the effective thermal conductivity of the saturated sediment is defined as $\lambda^* = \lambda_f^{\phi} \lambda_s^{(1-\phi)}$, where λ_f and λ_s are the thermal conductivities of water and the sediment grains, respectively, then the effective thermal diffusivity can be written.

$$\kappa_e = \frac{\lambda^*}{C} + D_{eff} \tag{3}$$

where D_{eff} is the effective dispersion coefficient. Introducing D_{eff} provides a way to increase the rate of heat transport, imitating the rapid heat transport that in reality is a product of 3-D hydrodynamic exchange. Bhaskar et al. (2012) imposed a constant value of D_{eff} down to a specified depth, below which D_{eff} was zero. Analytical solutions suggest that hydrodynamic exchange driven by waves and flow over ripples decays exponentially below the sediment–water

interface (Elliott and Brooks, 1997; Qian et al., 2008). Other studies have shown that a corresponding exponential decay in D_{eff} reproduces field (Jahnke et al., 2005) and laboratory (Qian et al., 2009) observations, using

$$D_{eff} = D_o e^{-kz} \tag{4}$$

where k is

$$k = \frac{\ln(2)}{d_{1/2}} \tag{5}$$

and $d_{1/2}$ is the half-depth, which is the depth below the sediment–water interface at which $D_{eff} = D_o/2$. It is also convenient to define a non-dimensional thermal diffusivity index

$$TDI = \frac{D_{eff}}{(\lambda^*/C)} \tag{6}$$

As discussed by Bhaskar et al. (2012), when $TDI < 0.3$, heat conduction dominates diffusive heat transfer; when $TDI > 3$, dispersion dominates diffusive heat transfer. Thus TDI > 3 indicates rapid hydrodynamic exchange. Time-series profiles of TDI reveal the timing, degree, and depth of rapid hydrodynamic exchange. Estimating the flux of fluid that is required to create the thermal signal is an obvious next step but is a large enough step that it is beyond the scope of the current paper. The primary goal of the current paper is to determine the timing and extent of rapid hydrodynamic exchange.

Many studies have inverted thermal time series data in a 1-D framework to determine v. Analytic solutions of (1) have been widely used to determine groundwater velocity below streams (Anibas et al., 2011; Briggs et al., 2012; Irvine and Lautz, 2015; Irvine et al., 2015). Computer codes are now available that greatly simplify these analyses (Gordon et al., 2012; Swanson and Cardenas, 2011), and, Schmidt et al. (2014) developed models to allow automated estimation of time-varying v in systems described by (1). These 1-D methods are also increasingly accompanied by more complex two-dimensional coupled models of groundwater flow and heat transport (Nützmann et al., 2014; Rahimi et al., 2015).

In contrast to methods that are designed to obtain v, methods for analyzing hydrodynamic exchange are in general far more complex. With the exception of Bhaskar (2012), models of hydrodynamic exchange have commonly coupled surface water flow with groundwater flow in two- and three-dimensional systems (Cardenas and Wilson, 2007; Hester et al., 2009; Janssen et al., 2012; Menichino and Hester, 2014; Sawyer and Cardenas, 2009). This difference in approach is caused to some extent by different goals, particularly questions about how hydrodynamic exchange influences thermal regimes that affect ecosystem functions, rather than questions about the depth of the zone of hydrodynamic exchange (e.g. Cardenas and Wilson, 2007; Sawyer et al., 2012). These models can clearly be used to determine the depth of hydrodynamic exchange, but they are much more computationally demanding than the simple 1-D approaches that have been so widely used in the heat tracer literature. The purpose of the current paper is to present a new model that was designed to estimate the time-varying depth of hydrodynamic exchange using a simple and efficient 1-D framework.

3. Methods

3.1. Numerical method

We developed a new computer program, the Model for Advanced Thermal Time-Series Inversion (MATTSI), to estimate the depth and extent of hydrodynamic exchange below the sediment–water interface in systems that can also include regional groundwater flow. The model is written in MATLAB. Input is entered by editing a well-commented text file. In MATTSI, (1) is solved using a 1-D Galerkin finite element method. The temperature at the upper boundary is specified using observed temperatures from the surface water. The temperature at the lower boundary is also specified. The depth of the simulation domain is set by the user in the input file, but the program is currently designed for the simulation domain to extend 10 m below the sediment–water interface, which is deep enough that seasonal temperature variations are small. Thus the temperature at the lower boundary is specified to be the average annual temperature. Initial conditions can be entered by the user or generated using an analytic solution included in the model that assumes sinusoidal seasonal variations in temperature at the seafloor (Carslaw and Jaeger, 1959, Section 2.6).

MATTSI nests this 1-D heat transport model inside a larger MATLAB script that uses the fmincon function for constrained minimization to minimize the root mean squared error (RMSE) between simulated and observed temperatures. The program finds optimized pairs of D_o and $d_{1/2}$. The user supplies upper search bounds for D_o and $d_{1/2}$ and sets optimization tolerances (stopping criteria) required for the minimization routine (Table 2). The groundwater flow velocity is specified by the user rather than being part of the optimization routine because, although it is unlikely to be known *a priori*, it is assumed to remain relatively constant over observation periods of a few weeks. Thus is it reasonable to test different values for v in separate runs, rather than attempting three-parameter estimation. Minimization is applied sequentially to segments of the dataset, which are referred to as optimization intervals. The length of the optimization interval is specified by the user in the input file. Final temperatures from each optimization interval are passed to the next optimization interval as initial conditions. Additional parameters necessary to solve (1) are listed in Table 3.

The program returns the *TDI* and simulated T as a function of depth and time at the end of each optimization interval. As will be shown below, TDI provides a clear visual indication of the timing and depth of hydrodynamic exchange, because TDI > 3 stands out visually against a background of TDI < 1 in plots of TDI. Time-

Table 2
Optimization parameters and sensitivity studies.

Parameter definition	Value for field example
Function tolerance	10^{-6}
Vector tolerance	10^{-6}
Maximum $\frac{D_o}{\lambda^*}$	500
Maximum $d_{1/2}$	0.01, 0.02, 0.04, 0.06, 0.10, 0.15 m
Optimization interval	2, 4, 6, 10, 15, 20, 30 min

Table 3
Parameters for the heat transport model.

Parameter	Definition	Value	Units
ϕ	Porosity	0.40	(–)
ρ_f	Density of seawater	1025	kg m^{-3}
ρ_s	Density of sediment grains	2650	kg m^{-3}
c_f	Specific heat capacity of seawater	3993	J kg^{-1} K^{-1}
c_s	Specific heat capacity of sediment grains	1170	J kg^{-1} K^{-1}
λ^*	Effective thermal conductivity	1.57[a], 2.00[b]	W m^{-1} K^{-1}
v	Vertical groundwater flow rate[c]	3[a], 1.5[b]	m yr^{-1}

[a] Synthetic test case.
[b] Field cases.
[c] Positive numbers indicate upward flow.

series analysis is often desirable for identifying periodicity in hydrodynamic exchange, and this process is greatly simplified when the results can be distilled into a single number for each optimization interval. It is possible to use TDI from a single depth for time series analysis, but this excludes information from all other depths. Instead, MATTSI calculates the depth integral of D_{eff}, to obtain

$$D_{int} = \int_0^\infty D_{eff}\,dz = \int_0^\infty D_o e^{-kz}\,dz = \frac{D_o}{k} = \frac{D_o d_{1/2}}{\ln(2)} \quad (7)$$

Because D_{int} is the integral of D_{eff} over the entire simulation domain for a given time step, periods with significant hydrodynamic exchange will have a high D_{int}, and periods with little hydrodynamic exchange will have a low D_{int}. Visual comparisons of TDI and D_{int} confirm that D_{int} provides a reliable index of the timing and degree of hydrodynamic exchange events for time-series analysis. RMSE is also calculated at the end of each optimization interval by comparing the simulated thermal profile to the observed temperatures that correspond to that time step. To allow for quick comparisons of many simulations, we also report the average RMSE and average D_{int} for each simulation.

3.2. Datasets

We tested MATTSI using a synthetic dataset and two field datasets (Fig. 1). All datasets show tidal variations in temperature at the seafloor superimposed on longer warming and cooling trends. The tidal variations in the field data occur because warm coastal water moves seaward during ebb tide, and cooler offshore water moves landward during flood tide. Diurnal variations in temperature, as commonly seen in streams, are negligible compared to tidal variations in temperature. Longer warming and cooling trends reflect episodic intrusion of cold water onto the shelf from offshore. All datasets show temperatures at 0, 3, 6, 9 and 12 cm below the seafloor.

The synthetic dataset was generated by solving (1) while allowing the temperature at the seafloor to vary according to

$$T_{sf} = T_{avg} + A_1 \sin\left(\frac{2\pi t}{k_1}\right) + A_2 \sin\left(\frac{2\pi t}{k_2}\right) \quad (8)$$

where T_{sf} is the temperature at the seafloor, T_{avg} is the average temperature (here, 26 °C), A is the amplitude, t is time, and k is the period. We set A_1 and A_2 to be 0.25 °C and 1 °C, respectively; k_1 and k_2 were 12 h and 250 h (10.4 days). The period of 250 h for k_2 allowed us to include a cooling trend, a warming trend, and a short repeated section of the signal in a short (two-week) simulation. Hydrodynamic exchange was imposed for a four-hour period every 10 h, so that hydrodynamic exchange would affect different segments of the tidal signal. We set $d_{1/2}$ = 5 cm, which caused hydrodynamic exchange to die out by approximately 25 cm (five half-depths), similar to field and laboratory observations (Huettel et al., 2014; Jahnke et al., 2005). We set D_o to vary sinusoidally, with a maximum of 150 λ^* and a minimum of zero (Fig. 2b). Using (7), the peak D_{int} was 3.1 cm^3/s. The average linear velocity of the groundwater was 3.0 m/yr upward. Additional heat transport parameters used to solve (1) are listed in Table 3.

The field datasets were collected from a site 50 km offshore of St. Catherine's Island, GA (31°22.5N, 80°34.0W; Fig. 2) during the summer of 2008 (Savidge et al., in press). The ocean is 27 m deep at the site. Sonar images and diver observations during the summer of 2008 indicate a ripple field with a wavelength of approximately 0.75 m and an amplitude of no more than a few cm (Savidge et al., in press). Temperature was recorded at 1 min intervals using a string of BetaTHERM 100K6A11A thermistors coupled to a Campbell Scientific CR1000 Measurement and Control Module. The thermistors were accurate to ±0.1 °C, with resolution of 0.06 °C. Sensors were placed 10 cm above the seafloor and 3, 6, 9, and 12 cm below the sediment–water interface inside a CPVC tube with holes drilled at the sensor locations. The inside of the tube was filled with non-conductive epoxy.

Temperature was recorded from June 20 to July 9 and July 11 to August 7, 2008. A sudden change in the character of the thermal records suggested that sediments were scoured from the site on June 28, so that the second sensor likely recorded bottom water temperature until the instrument was retrieved on July 9. The depth of scour was uncertain, so our analysis of the first deployment focuses on June 20–28. Comparisons with a bottom mooring 1 km away indicated that the temperature recorded by the bottom water sensor began to drift midway through the second deployment, so a linear drift correction was applied from July 14 through

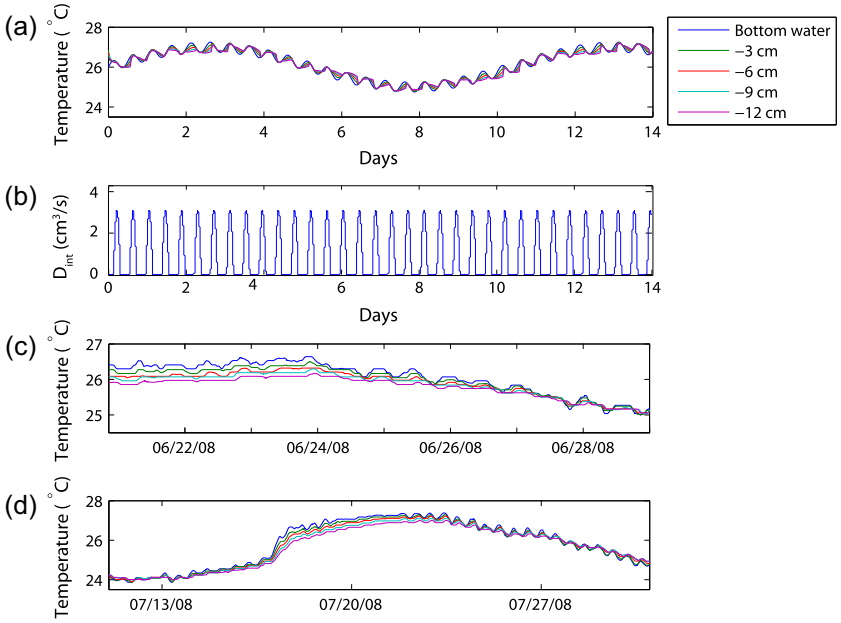

Fig. 1. Temperature datasets. (a) Synthetic dataset. (b) D*int* used to generate the synthetic dataset. Maximum *Dint* was 3.1 cm^3/s. (c) Field dataset from June to July 2008. (d) Field dataset from July to August 2008.

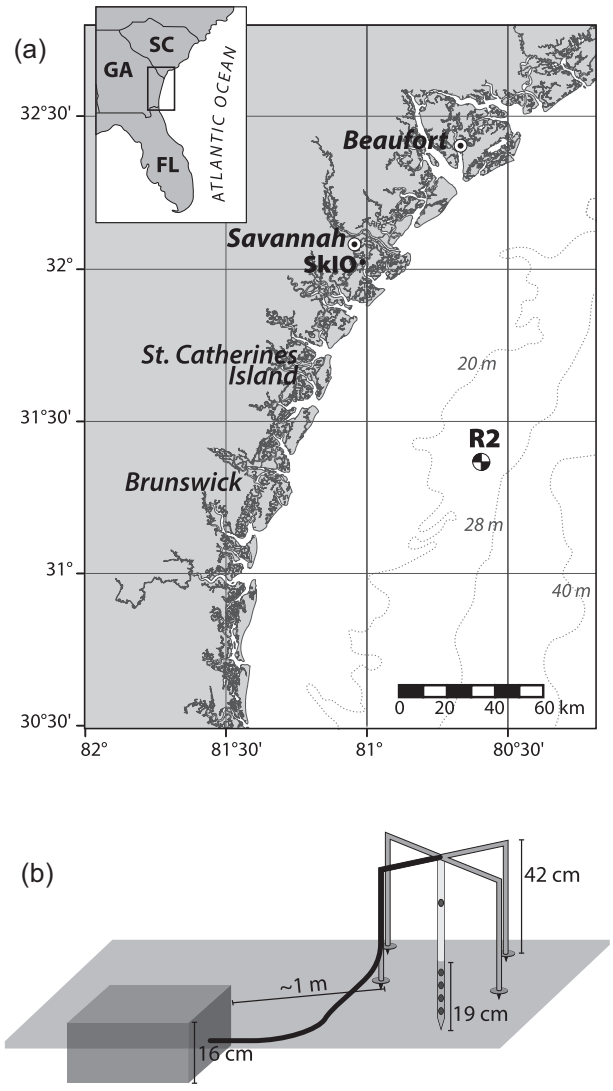

Fig. 2. Field map (a) and instrument (b). SC = South Carolina, GA = Georgia, FL = Florida.

July 30. The instrument had failed at all depths by the time it was retrieved in August. At retrieval it was clear that the housing had come apart and let seawater into the instrument; the temperature data indicate that this breakdown probably began on July 31, so the remaining data were discarded. The data were smoothed using a 2-h running average to remove numerical chatter (discrete steps of 0.06 °C, the resolution of the instrument) prior to their use in the numerical model.

The field dataset presented here is limited in depth. Periods where all four subsurface thermistors register the same temperature suggest that hydrodynamic exchange extended below the 12 cm monitored section (Fig. 1c and d). Given this limitation, it was not obvious at the outset whether the depth of hydrodynamic exchange could be determined uniquely or whether models using this dataset would be sensitive to v. Part of our test of the method was to see how much information can be extracted from a shallow dataset.

3.3. Numerical models

We used MATTSI to invert the synthetic and field datasets. In these models we used a simulation domain that reached from the seafloor to 10 m below the seafloor, a depth that is not affected by seasonal variations in ocean temperature. Grid discretization ranged from 0.003 m at the seafloor to 0.25 m at depth. Initial conditions for the synthetic dataset were generated using an analytical solution, as described above. Initial conditions for the field dataset were generated by running the 1-D heat transport model forward for the six months prior to the subseafloor monitoring period, using bottom water temperatures from a nearby mooring and setting v and D_o to zero. As shown below, the MATTSI simulations were not significantly affected by the choice of initial conditions beyond an initial ~3 day equilibration period. Within each optimization interval, the time step for the 1-D thermal model was 1 min. Using a shorter time step did not change the results.

Optimization tolerances for the optimization variables (D_o and $d_{1/2}$) and optimization output (RMSE) were set to 10^{-6}. Looser tolerances generated smoother results, but semi-diurnal peaks tended to smooth into single diurnal peaks. Tighter tolerances increased run times without changing the periodicity of the output. The target RMSE for the field data was 0.03 or less, because the resolution of the thermal data was 0.06 °C.

We conducted several sensitivity studies. The most important of these focused on choosing the upper search bounds for D_o and $d_{1/2}$, because it quickly became clear that, above a certain threshold, many values of D_{int} could generate similar, acceptable RMSEs. We noted that Jahnke et al. (2005) estimated D_o was 250 times the diffusion coefficient at a nearby site on the Ga. shelf; we found that once D_o was 200 λ^*, further increases made little difference. Thus we capped the search range for D_o at 500 λ^* for all sensitivity studies and focused on varying the cap for $d_{1/2}$. We tested a range of optimization intervals from 2 min to 45 min. We also tested the sensitivity of the model to v, λ^*, and errors in sensor depth.

4. Results

Initial simulations that did not allow hydrodynamic exchange but tried a very wide range for v confirmed that neither of the field datasets could be reproduced without adding effective dispersion (Fig. S1). Model runs based on the synthetic dataset clearly identified periods of hydrodynamic exchange (Fig. 3). Recall that the synthetic dataset was generated using $d_{1/2}$ = 0.05 m, and the peak D_{int} was 10.8 W K^{-1}. Results from runs with $d_{1/2}$ capped at 0.04 and 0.06 m are shown to illustrate the behavior of the model when the cap for the half-depth is higher or lower than the actual half depth. The D_{int} output (Fig. 3b–d) was noisy compared to the input signal (Fig. 1b) but clearly recognizable in both runs. When $d_{1/2}$ was capped at 0.04 m, the average RMSE was 0.0022 °C, less than 1% of the thermal amplitude associated tidal fluctuations. The magnitude of hydrodynamic exchange, as judged by peak D_{int}, was accurate to within a factor of two of the target D_{int}, indicating that the total amount of dispersion estimated by the model for each optimization interval was accurate to within a factor of two. When the cap for $d_{1/2}$ was raised to 0.06 m, the D_{int} signal remained very similar, but the ability to add slightly more dispersion allowed the average RMSE to fall to 0.0012 °C. As discussed further below, errors rose when the cap on $d_{1/2}$ was set too low, because the simulation could not add enough dispersion to match the observations.

A few spikes developed in the D_{int} signal at approximately 3, 10.5, 11 and 13 days in the simulation when $d_{1/2}$ was capped at 0.04 m (Fig. 3c). These spikes were associated with "false flushing events" that developed during brief instances when the subsurface was isothermal purely through conduction (gray arrows in Fig. 3a). This effect was greatly reduced when the cap was raised to 0.06 m (spike at 11 days only, Fig. 3d). These events typically did not affect the RMSE significantly (Fig. 3e). Note also that the very brief spikes of added dispersion did not perturb the simulated temperatures

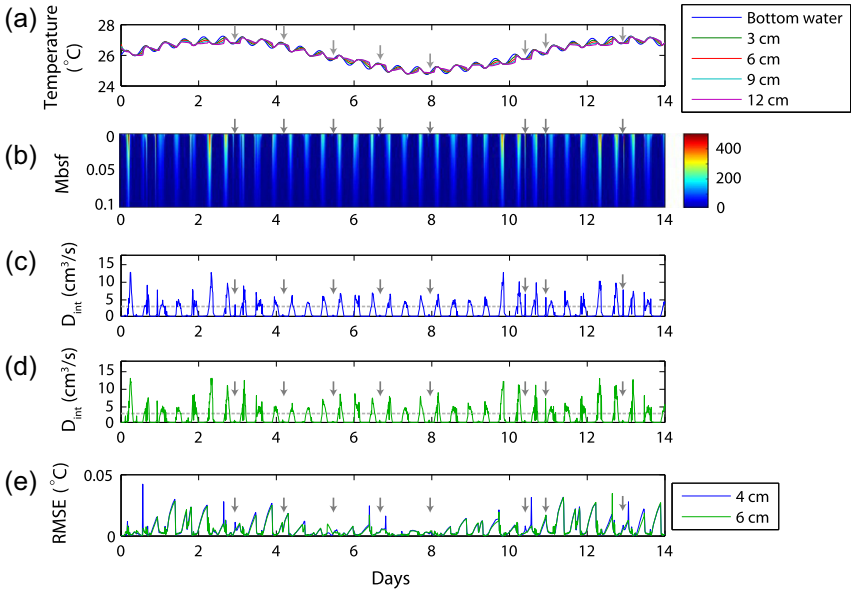

Fig. 3. Model inversion results for the synthetic dataset. (a) Original dataset. (b)TDI when $d_{1/2}$ was capped at 4 cm. Mbsf indicates meters below the seafloor. (c) D_{int} when $d_{1/2}$ was capped at 4 cm. Dashed gray line indicated maximum Dint of the input signal (Fig 1b), 3.1 cm^3/s. (d) D_{int} when $d_{1/2}$ was capped at 6 cm. (d) RMSE. Gray arrows indicate times when conduction caused isothermal conditions (a) and the model response (b–e).

significantly in the uppermost 12 cm, because the temperatures were already very close to isothermal.

In both of the simulations shown in Fig. 3, the model systematically estimated higher degrees of hydrodynamic exchange than occurred in the input signal (Fig. 1b) when tidal variations in temperature and longer thermal trends moved in opposite directions, for example, when tidal warming was superimposed on longer cooling trends. These systematic errors likely reflect a slight lag in detecting hydrodynamic exchange. For tidal warming, a slight lag allows the bottom water temperature to cool somewhat by the time the model imposes hydrodynamic exchange. More dispersion is then required to achieve the correct degree of warming. When the tidal and longer-term thermal trends moved in the same direction, less dispersion was necessary to move the required amount of heat. Although errors were very small, the RMSE increased during times when D_{int} was overestimated (e.g., days 1–4 vs. days 5–8).

We ran simulations with different optimization intervals to see how errors, including lags in detecting hydrodynamic exchange, were affected (Fig. 4). Simulations with optimization intervals of less than 10 min responded quickly to small variations, which produced somewhat noisy results from a smooth input signal. There was little significant change in the timing or relative height of peaks in D_{int}, but the extra activity caused the average D_{int} and average RMSE to rise (Fig. 4). Simulations with optimization intervals ranging from 10 to 30 min produced results that were very similar to one another, with low average D_{int} and RMSE. The similarity between the results using 10-min and 30-min optimization intervals suggests that the lag in detecting flushing was not related to temporal resolution. A more likely cause of the lag is that MATTSI is not very sensitive to low levels of hydrodynamic exchange, such as may occur at the beginning or end of exchange events. Increasing the optimization interval beyond about 30 min caused the average RMSE to rise, because the interval was too long to accurately sample the tidally-influenced dataset.

We ran a series of simulations with the same optimization interval but different upper bounds for $d_{1/2}$ to test the model's ability to identify the half-depth of hydrodynamic exchange. Comparisons revealed a trough in D_{int} and RMSE when $d_{1/2}$ was capped at

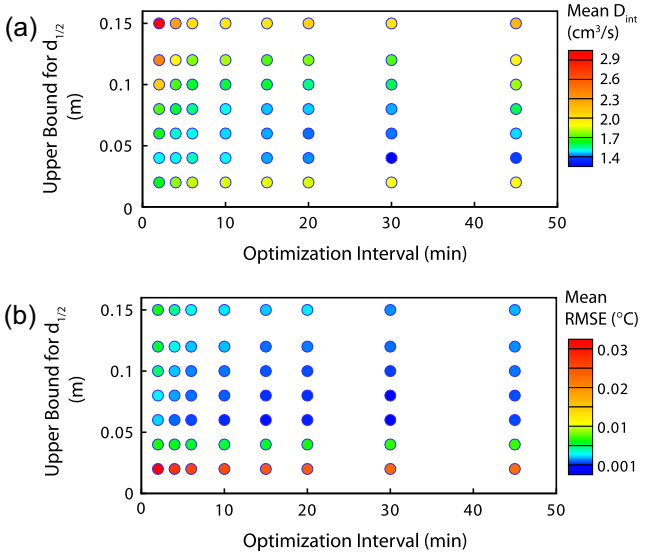

Fig. 4. Sensitivity studies. (a) Grid showing the average D_{int} calculated for 56 simulations that were run with optimization intervals ranging from 2 to 45 min and a range of upper bounds for $d_{1/2}$ (2–15 cm). (b) RMSE for the same simulations as (a). Note lowest contour in (b) is 0.001 °C rather than 0.0 °C.

0.06 m (Fig. 4). These results confirm that capping $d_{1/2}$ below the value used in generating the dataset increased errors, because too little hydrodynamic exchange was allowed. In simulations where the cap for $d_{1/2}$ was set significantly higher than the actual value, the code tended to "overshoot," i.e. impose hydrodynamic exchange to greater depths than necessary. This occurred because our test was designed to mimic our field datasets, which were very shallow and therefore lacked the deeper temperature constraints that would have prevented overshoot. Overshoot was, however, revealed by a rise in RMSE, because extra hydrodynamic exchange imposed during one time step caused errors in subsequent time steps. Thus, although the dataset was shallow and the program returns TDI rather than $d_{1/2}$, the method can be used to identify the approximate half-depth of hydrodynamic exchange.

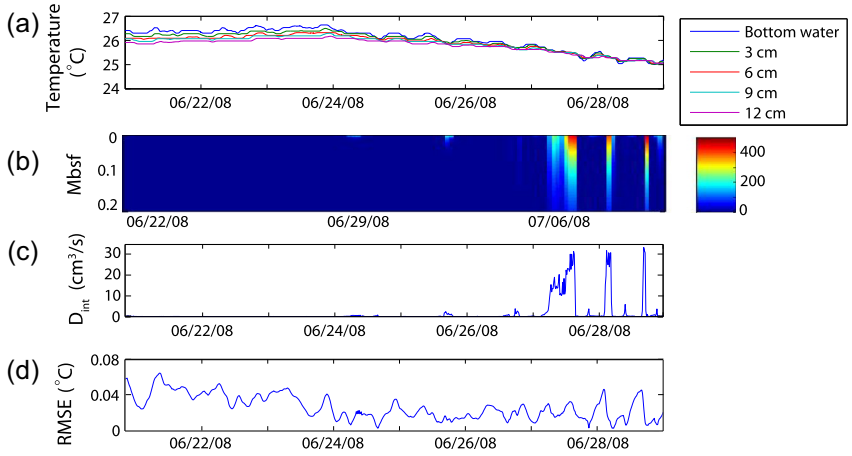

Fig. 5. Model inversion results for the first (June) field monitoring dataset, when $d_{1/2}$ was capped at 8 cm. (a) Original dataset. (b) TDI. Mbsf indicates meters below the seafloor. (c) D_{int}. (d) RMSE.

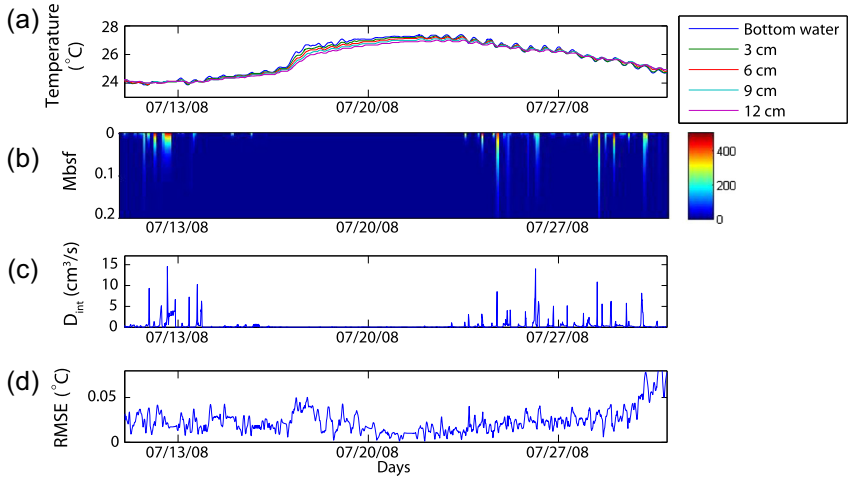

Fig. 6. Model inversion results for the second (July) field monitoring dataset, when $d_{1/2}$ was capped at 8 cm. (a) Original dataset. (b) TDI. Mbsf indicates meters below the seafloor. (c) D_{int}. (d) RMSE.

The model performed well when applied to the first (June 2008) field dataset, showing consistent patterns of episodic hydrodynamic exchange and average RMSEs below our target of 0.03 °C (Fig. 5). Little benthic exchange occurred before June 27. As further discussed by Savidge et al. (in press), time series analysis of the rest of the record indicated hydrodynamic exchange with weak semi-diurnal (tidal) and quarter-diurnal (semi-tidal) periodicity. This periodicity suggests that hydrodynamic exchange was triggered by current flow over the ripple field at the site. Hydrodynamic exchange was stronger on flood tide, however, despite tidally-symmetrical currents, and not all instances of high tidal current velocity caused hydrodynamic exchange. Rather, exchange appears to have been triggered by the combination of high tidal current velocities and thermal instability, which developed when the temperature of the bottom water fell below that of the porewater. Thermal instability would enhance hydrodynamic exchange on flood tide, when cooler offshore water migrated landward, and explains the lack of apparent hydrodynamic exchange during warming trends. The second deployment showed very similar results, wherein benthic exchange occurred with roughly tidal periodicity during cooling trends but was damped during a warming trend July 14–22 (Fig. 6).

As we did with the synthetic dataset, we tested many combinations of upper bounds for D_o and $d_{1/2}$. Again we found that optimal solutions minimized both RMSE and D_{int}. The optimal upper bound for $d_{1/2}$ was found to be 0.08 m for both field deployments (Fig. 7). Given that D_{eff} decays to 3% of its maximum after five half-depths, this suggests significant hydrodynamic exchange in the upper ~25 cm of the sediment column. An investigation of the effect of the optimization interval for the first deployment confirmed that an optimization interval of 15–20 min is appropriate. Longer optimization intervals showed lower average RMSEs, but the amount of added effective dispersion increased substantially (Fig. 7c and d). Shorter optimization intervals allowed the simulation to respond quickly to small changes, including sensor noise. This quick response reduced the amount of added dispersion in the simulation, but caused significant increases in the RMSE (Fig. 7c and d). The second deployment showed the same patterns and confirmed that the timing of hydrodynamic exchange identified by the program remained similar over a wide range of optimization intervals (Fig. S2).

The models were able to constrain the groundwater flow rate, v, somewhat better than expected. It was not possible to distinguish between, for example, 0 m/yr and 3 m/yr (upward or downward). This is consistent with thermal Pe number calculations (ratio of advective flux to conductive flux; Anderson, 2005), which suggest that such low flow rates are at or below the detection limit for heat tracers. The RMSE increased as $|v|$ rose beyond 3 m/yr. Better

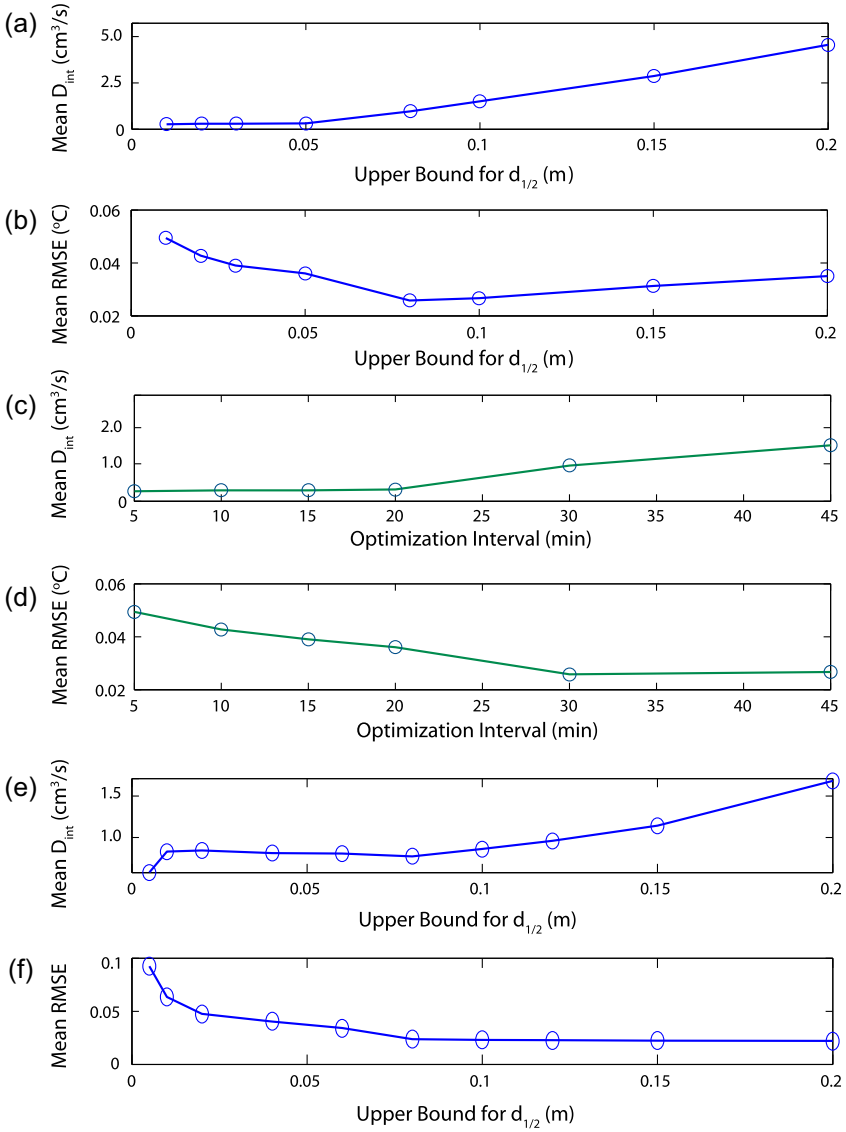

Fig. 7. Sensitivity studies. (a) Mean D_{int} calculated using a range of upper limits for $d_{1/2}$ when the optimization interval was 15 min for the June dataset. (b) Mean RMSE calculated using a range of upper limits for $d_{1/2}$ when the optimization interval was 15 min for the June dataset. (c) Mean D_{int} for a range of optimization intervals when the upper limit for $d_{1/2}$ was set to 0.08 m for the June dataset. (d) Mean RMSE for a range of optimization intervals when the upper limit for $d_{1/2}$ was set to 0.08 m for the June dataset. (e) Mean D_{int} calculated using a range of upper limits for $d_{1/2}$ for the July dataset (optimization interval = 15 min). (f) Mean RMSE calculated using a range of upper limits for $d_{1/2}$ for the July dataset (optimization interval = 15 min).

estimates of v will require observations from greater depths than 12 cm, but the fact that groundwater flow rates can be constrained to $|v| \leqslant 3$ m/yr using such shallow data is a useful result.

5. Discussion

We tested many aspects of the model to determine how sensitive it was to errors in input parameters. As previously indicated, the model was not very sensitive to small (<3 m/yr) variations in v. An optimal v could have been declared based on small variations in the average RMSE between simulations with $|v| \leqslant 3$ m/yr, but given that all of the average RMSEs in question were less than 50% of the instrument resolution, the differences cannot be said to be significant. Moreover, the timing and relative heights of the peaks in D_{int} remained very similar. Changes in λ^* similarly failed to produce large changes in D_{int}, although increasing λ^* from 1.6 to 2.0 W m^{-1} K^{-1} did reduce the average RMSE slightly. A realistic range of porosity values caused similarly small changes to D_{int}. The model was also relatively insensitive to the way decreases in D_{eff} with depth were parameterized. We experimented with constant D_{eff}, linearly-declining D_{eff}, and the exponential model. All produced similar patterns of hydrodynamic exchange, so we proceeded with the exponential model, which has the strongest theoretical underpinning. Overall, the timing and magnitude of hydrodynamic exchange determined by the inversion routine are not very sensitive to uncertainty in physical input parameters (v and λ^*), although RMSE increases as these parameters diverge from realistic values. Results were also insensitive to errors of 1 cm in sensor depth (Fig. S3), even in a system where the shallowest sensor was deployed only 3 cm below the sediment–water interface. The method is therefore likely to be useful in systems with deployment errors, migrating ripples, and, to a degree, scour. Overall, the single most important control on the timing and depth of hydrodynamic exchange identified by the model was whether the input temperature signal conformed to conductive flow patterns.

It is reasonable to consider whether time-varying v rather than hydrodynamic dispersion could explain the field datasets. We rejected this possibility because, when the observed temperature

signal deviated from simple heat conduction, it always did so in the same way. That is, the temperature in the sediments collapsed toward the temperature of the ocean bottom water, indicating rapid influx of seawater. This occurred on rising and falling tides. There is no obvious mechanism for groundwater flow that would drive downward v on rising and falling tides. Tidal fluctuations certainly cause groundwater velocities to change in coastal systems, but they drive flow in opposite directions during rising and falling tides. The simplest explanation is that the signal was caused by hydrodynamic exchange, which can logically drive seawater through seafloor sediments on rising and falling tides.

The results presented above show that the model can identify transient hydrodynamic exchange. This is clearly necessary in tidally-influenced systems, including tidal creeks and shallow continental shelves; the method can also be applied to streams that experience rapid changes in discharge. The model does not, however, identify the causes of hydrodynamic exchange. The causes are instead inferred based on the timing of hydrodynamic exchange events and their correspondence with other environmental variables. The degree of additional data collection required to characterize these additional environmental variables depends on the system of interest. In streams where rating curves have been developed, knowledge of the depth and temperature of the surface water is likely sufficient to distinguish between current-driven flow and thermal overturn. The relationship between tidal currents and the depth of surface water is more complex in tidal channels, where the problem of bi-directional flow is compounded by significant variations in mean water level (sea level averaged over one or more tidal cycles) and tidal amplitude. In tidal systems, it will be necessary to monitor current velocity and temperature.

The current approach is limited to some degree because the user chooses the search range for the half-depth, and this search range remains the same for the entire simulation. This approach worked well for the datasets presented here, but no major storm events occurred during the observation period. Storms have the potential to induce hydrodynamic exchange to depths of meters (Moore and Wilson, 2005). We recommend that periods with dramatic shifts in forcing factors be analyzed separately from the surrounding "normal" conditions, to determine appropriate search bounds for the different conditions. A first-pass way to identify periods that require different search bounds or other adjustments is to run the entire dataset and look for sustained intervals with elevated RMSE.

Finally, the assumption that D_{eff} declines exponentially with depth below the sediment–water interface also assumes homogeneous sediments. Among broad sediment types, sandy continental shelf sediments are likely to be reasonably homogeneous (Wilson et al., 2008), but streambed sediments may be highly heterogeneous. Layers of fine-grained sediments may also be present in continental shelf environments. We suggest that D_{eff} be set to zero below the top of any low-permeability layer, because laboratory studies suggest that hydrodynamic exchange is significantly reduced below a permeability of approximately 10^{-12} m^2 (Huettel et al., 2014). Sediment compaction can also cause the permeability of sediments to decline with depth, but sandy sediments of the type that are likely to be affected by hydrodynamic exchange are not compressible enough for permeability to be affected significantly in the upper meter or two of seafloor sediments. We also note that the depth of hydrodynamic exchange may vary spatially in response to seafloor features like ripples. It is not possible to say whether this issue affected the data reported in this paper, although it should be noted that the timing of flushing events identified by the model are unlikely to be affected. Future investigations should consider installing multiple instruments across ripple beds to determine the importance of this kind of variation.

6. Conclusion

This work demonstrates that it is possible to determine the depth and intensity of transient hydrodynamic exchange by inverting thermal observations. The MATTSI computer program, currently written in MATLAB, can be used to estimate the depth and extent of hydrodynamic exchange below a sediment–water interface. Slight delays in detecting flushing can lead to errors of approximately a factor of two, as measured by integrating the addition of effective dispersion over the depth, but the overall timing and extent of hydrodynamic exchange events were clearly indicated through a wide range of sensitivity studies. In particular, the results were relatively insensitive to uncertainty in the installation depth of sensors and in the effective thermal conductivity of the sediments, both of which are commonly somewhat difficult to establish with precision in field deployments. We found that it was possible to identify the depth of flushing using shallow datasets, in which flushing extended below the deepest sensor. It is recommended, however, that future monitoring programs install sensors to greater depths to prevent model overshoot. In the field example tested here, results suggest that monitoring to 50 cm would have been sufficient. The model suffers from an inability to distinguish very low (<3 m/yr) groundwater flow velocities, a problem common to all methods that rely on heat as a tracer.

Acknowledgments

We thank Anna Boyette for help with the figures and Dan Rosenberry for tipping us off to the term "hypolentic." Readers are invited to express their approval, disapproval, or outright rejection of the term "hypokymatic" in their future publications. MATTSI is freely available at www.geol.sc.edu/MATTSI. We thank three anonymous reviewers whose comments significantly improved the presentation of this work. This material is based upon work supported by the National Science Foundation under Grants EAR-1316250 (AMW) and OCE-0536326 (WBS). Any opinions, findings, and conclusions or recommendations expressed in this material are those of the authors and do not necessarily reflect the views of the National Science Foundation.

Appendix A. Supplementary material

Supplementary data associated with this article can be found, in the online version, at http://dx.doi.org/10.1016/j.jhydrol.2016.04.047.

References

Anderson, M.P., 2005. Heat as a ground water tracer. Ground Water 43, 951–968. http://dx.doi.org/10.1111/j.1745-6584.2005.00052.x.

Anibas, C., Buis, K., Verhoeven, R., Meire, P., Batelaan, O., 2011. A simple thermal mapping method for seasonal spatial patterns of groundwater–surface water interaction. J. Hydrol. 397, 93–104. http://dx.doi.org/10.1016/j.jhydrol.2010.11.036.

Aseltyne, T.A., Rowe, H.D., Fryar, A.E., 2006. Stable isotopic fingerprint of a hyporheic–hypolentic boundary in a reservoir. Hydrogeol. J. 14, 1688–1695. http://dx.doi.org/10.1007/s10040-006-0088-2.

Befus, K.M., Cardenas, M.B., Erler, D.V., Santos, I.R., Eyre, B.D., 2013. Heat transport dynamics at a sandy intertidal zone. Water Resour. Res. 49, 3770–3786. http://dx.doi.org/10.1002/wrcr.20325.

Bethke, C.M., 1985. A numerical model of compaction-driven groundwater flow and heat transfer and its application to the paleohydrology of intracratonic sedimentary basins. J. Geophys. Res. 90, 6817–6828.

Bhaskar, A.S., Harvey, J.W., Henry, E.J., 2012. Resolving hyporheic and groundwater components of streambed water flux using heat as a tracer. Water Resour. Res. 48, W08524. http://dx.doi.org/10.1029/2011WR011784.

Boano, F., Harvey, J.W., Marion, A., Packman, A.I., Revelli, R., Ridolfi, L., Wörman, A., 2014. Hyporheic flow and transport processes: mechanisms, models, and biogeochemical implications. Rev. Geophys. 52, 603–679. http://dx.doi.org/10.1002/2012RG000417.

Boano, F., Poggi, D., Revelli, R., Ridolfi, L., 2009. Gravity-driven water exchange between streams and hyporheic zones. Geophys. Res. Lett. 36, 1–5. http://dx.doi.org/10.1029/2009GL040147.

Bredehoeft, J.D., Papadopulos, I.S., 1965. Rates of vertical groundwater movement estimated form the earth's thermal profile. Water Resour. Res. 1, 325–328.

Briggs, M.A., Lautz, L.K., McKenzie, J.M., Gordon, R.P., Hare, D.K., 2012. Using high-resolution distributed temperature sensing to quantify spatial and temporal variability in vertical hyporheic flux. Water Resour. Res. 48, 1–16. http://dx.doi.org/10.1029/2011WR011227.

Brunke, M., Gonser, T., 1997. The ecological significance of exchange processes between rivers and groundwater. Freshw. Biol. 37, 1–33. http://dx.doi.org/10.1046/j.1365-2427.1997.00143.x.

Burnett, W.C., Bokuniewicz, H., Huettel, M., Moore, W.S., Taniguchi, M., 2003. Groundwater and pore water inputs to the coastal zone. Biogeochemistry 66, 3–33.

Cardenas, M.B., Wilson, J.L., 2007. Effects of current-bed form induced fluid flow on the thermal regime of sediments. Water Resour. Res. 43, W08431. http://dx.doi.org/10.1029/2006WR005343.

Carslaw, H., Jaeger, J., 1959. Conduction of Heat in Solids, second ed. Oxford University Press, New York.

Cho, Y.-M., Werner, D., Moffett, K.B., Luthy, R.G., 2010. Assessment of advective porewater movement affecting mass transfer of hydrophobic organic contaminants in marine intertidal sediment. Environ. Sci. Technol. 44, 5842–5848. http://dx.doi.org/10.1021/es903583y.

Conant, B., Cherry, J.A., Gillham, R.W., 2004. A PCE groundwater plume discharging to a river: influence of the streambed and near-river zone on contaminant distributions. J. Contam. Hydrol. 73, 249–279. http://dx.doi.org/10.1016/j.jconhyd.2004.04.001.

Constantz, J., 2008. Heat as a tracer to determine streambed water exchanges. Water Resour. Res. 44, W00D10. http://dx.doi.org/10.1029/2008WR006996.

Cook, P.L.M., fer, F.W., Glud, R.N., Janssen, F., Huettel, M., 2007. Benthic solute exchange and carbon mineralization in two shallow subtidal sandy sediments: effect of advective pore-water exchange. Limnol. Oceanogr. 52, 1943–1963. http://dx.doi.org/10.4319/lo.2007.52.5.1943.

Ehrenhauss, S., Huettel, M., 2004. Advective transport and decomposition of chain-forming planktonic diatoms in permeable sediments. J. Sea Res. 52, 179–197. http://dx.doi.org/10.1016/j.seares.2004.01.004.

Elliott, H., Brooks, N.H., 1997. Transfer of nonsorbing solutes to a streambed with bed forms : Theory, vol. 33, pp. 123–136.

Elliott, H., Brooks, N.H., Keck, W.M., 1997. Transfer of nonsorbing solutes to a streambed with bed forms: Laboratory experiments, vol. 33, pp. 137–151.

Gordon, R.P., Lautz, L.K., Briggs, M.A., McKenzie, J.M., 2012. Automated calculation of vertical pore-water flux from field temperature time series using the VFLUX method and computer program. J. Hydrol. 420–421, 142–158. http://dx.doi.org/10.1016/j.jhydrol.2011.11.053.

Harvey, J.W., Fuller, C.C., 1998. Effect of enhanced manganese oxidation in the hyporheic zone on basin-scale geochemical mass balance. Water Resour. Res. 34, 623–636. http://dx.doi.org/10.1029/97WR03606.

Hatch, C.E., Fisher, A.T., Revenaugh, J.S., Constantz, J., Ruehl, C., 2006. Quantifying surface water–groundwater interactions using time series analysis of streambed thermal records: method development. Water Resour. Res. 42. http://dx.doi.org/10.1029/2005WR004787, n/a–n/a.

Hester, E.T., Doyle, M.W., Poole, G.C., 2009. The influence of in-stream structures on summer water temperatures via induced hyporheic exchange. Limnol. Oceanogr. 54, 355–367. http://dx.doi.org/10.4319/lo.2009.54.1.0355.

Huettel, M., Berg, P., Kostka, J.E., 2014. Benthic exchange and biogeochemical cycling in permeable sediments. Ann. Rev. Mar. Sci. 6, 23–51. http://dx.doi.org/10.1146/annurev-marine-051413-012706.

Huettel, M., Rusch, A., 2000. Transport and degradation of phytoplankton in permeable sediment. Limnol. Oceanogr. 45, 534–549. http://dx.doi.org/10.4319/lo.2000.45.3.0534.

Huettel, M., Ziebis, W., Forster, S., 1996. Flow-induced uptake of particulate matter in permeable sediments. Limnol. Oceanogr. 41, 309–322. http://dx.doi.org/10.4319/lo.1996.41.2.0309.

Huettel, M., Ziebis, W., Forster, S., Luther, G.W.I., 1998. Advective transport affecting metal and nutrient distributions and interfacial fluxes in permeable sediments. Geochimica et Cosmochimica Acta 62, 613–631.

Irvine, D.J., Lautz, L.K., 2015. High resolution mapping of hyporheic fluxes using streambed temperatures: recommendations and limitations. J. Hydrol. 524, 137–146. http://dx.doi.org/10.1016/j.jhydrol.2015.02.030.

Irvine, D.J., Lautz, L.K., Briggs, M.A., Gordon, R.P., McKenzie, J.M., 2015. Experimental evaluation of the applicability of phase, amplitude, and combined methods to determine water flux and thermal diffusivity from temperature time series using VFLUX 2. J. Hydrol. 531, 728–737. http://dx.doi.org/10.1016/j.jhydrol.2015.10.054.

Jahnke, R., Richards, M., Nelson, J., Robertson, C., Rao, A., Jahnke, D., 2005. Organic matter remineralization and porewater exchange rates in permeable South Atlantic Bight continental shelf sediments. Cont. Shelf Res. 25, 1433–1452. http://dx.doi.org/10.1016/j.csr.2005.04.002.

Janssen, F., Cardenas, M.B., Sawyer, A.H., Dammrich, T., Krietsch, J., de Beer, D., 2012. A comparative experimental and multiphysics computational fluid dynamics study of coupled surface-subsurface flow in bed forms. Water Resour. Res. 48. http://dx.doi.org/10.1029/2012WR011982, n/a–n/a.

Janssen, F., Huettel, M., Witte, U., 2005. Pore-water advection and solute fluxes in permeable marine sediments (II): benthic respiration at three sandy sites with different permeabilities (German Bight, North Sea). Limnol. Oceanogr. 50, 779–792. http://dx.doi.org/10.4319/lo.2005.50.3.0779.

Jin, G., Tang, H., Li, L., Barry, D.A., 2011. Hyporheic flow under periodic bed forms influenced by low-density gradients. Geophys. Res. Lett. 38, 2–7. http://dx.doi.org/10.1029/2011GL049694.

King, J.N., Mehta, A.J., Dean, R.G., 2009. Generalized analytical model for benthic water flux forced by surface gravity waves. J. Geophys. Res. 114, C04004. http://dx.doi.org/10.1029/2008JC005116.

Laursen, A.E., Seitzinger, S.P., 2002. The role of denitrification in nitrogen removal and carbon mineralization in Mid-Atlantic Bight sediments. Cont. Shelf Res. 22, 1397–1416. http://dx.doi.org/10.1016/S0278-4343(02)00008-0.

Martin, J.B., Cable, J.E., Jaeger, J., Hartl, K., Smith, C.G., 2006. Thermal and chemical evidence for rapid water exchange across the sediment-water interface by bioirrigation in the Indian River Lagoon, Florida. Limnol. Oceanogr. 51, 1332–1341. http://dx.doi.org/10.4319/lo.2006.51.3.1332.

Menichino, G.T., Hester, E.T., 2014. Hydraulic and thermal effects of in-stream structure-induced hyporheic exchange across a range of hydraulic conductivities. Water Resour. Res. 50, 4643–4661. http://dx.doi.org/10.1002/2013WR014758.

Moore, W.S., 1999. The subterranean estuary: a reaction zone of ground water and sea water. Mar. Chem. 65, 111–125. http://dx.doi.org/10.1016/S0304-4203(99)00014-6.

Moore, W.S., 2010. The effect of submarine groundwater discharge on the ocean. Ann. Rev. Mar. Sci. 2, 59–88. http://dx.doi.org/10.1146/annurev-marine-120308-081019.

Moore, W.S., Krest, J., Taylor, G., Roggenstein, E., Joye, S.B., Lee, R., 2002. Thermal evidence of water exchange through a coastal aquifer : Implications for nutrient fluxes. Geophys. Res. Lett. 29, 2–5.

Moore, W.S., Wilson, A.M., 2005. Advective flow through the upper continental shelf driven by storms, buoyancy, and submarine groundwater discharge. Earth Planet. Sci. Lett. 235, 564–576. http://dx.doi.org/10.1016/j.epsl.2005.04.043.

Mulholland, P.J., Helton, A.M., Poole, G.C., Hall, R.O., Hamilton, S.K., Peterson, B.J., Tank, J.L., Ashkenas, L.R., Cooper, L.W., Dahm, C.N., Dodds, W.K., Findlay, S.E.G., Gregory, S.V., Grimm, N.B., Johnson, S.L., McDowell, W.H., Meyer, J.L., Valett, H. M., Webster, J.R., Arango, C.P., Beaulieu, J.J., Bernot, M.J., Burgin, A.J., Crenshaw, C.L., Johnson, L.T., Niederlehner, B.R., O'Brien, J.M., Potter, J.D., Sheibley, R.W., Sobota, D.J., Thomas, S.M., 2008. Stream denitrification across biomes and its response to anthropogenic nitrate loading. Nature 452, 202–205. http://dx.doi.org/10.1038/nature06686.

Nützmann, G., Levers, C., Lewandowski, J., 2014. Coupled groundwater flow and heat transport simulation for estimating transient aquifer-stream exchange at the lowland River Spree (Germany). Hydrol. Process. 28, 4078–4090. http://dx.doi.org/10.1002/hyp.9932.

Osborne, M., Swarbrick, R., 1997. Mechanisms for generating overpressure in sedimentary basins: a reevaluation. Am. Assoc. Pet. Geol. Bull. 81, 1023–1041.

Packman, A.I., Brooks, N.H., Morgan, J.J., 2000. A physicochemical model for colloid exchange between a stream and a sand streambed with bed forms. Water Resour. Res. 36, 2351–2361. http://dx.doi.org/10.1029/2000WR900059.

Precht, E., Franke, U., Polerecky, L., Huettel, M., 2004. Oxygen dynamics in permeable sediments with wave-driven pore water exchange. Limnol. Oceanogr. 49, 693–705. http://dx.doi.org/10.4319/lo.2004.49.3.0693.

Qian, Q., Clark, J.J., Voller, V.R., Stefan, H.G., 2009. Depth-dependent dispersion coefficient for modeling of vertical solute exchange in a lake bed under surface waves. J. Hydraul. Eng.

Qian, Q., Voller, V.R., Stefan, H.G., 2008. A vertical dispersion model for solute exchange induced by underflow and periodic hyporheic flow in a stream gravel bed. Water Resour. Res. 44, W07422. http://dx.doi.org/10.1029/2007WR006366.

Rahimi, M., Essaid, H.I., Wilson, J.T., 2015. The role of dynamic surface water-groundwater exchange on streambed denitrification in a forst-order, low-relief agricultural watershed [WWW Document]. Water Resour. Res. 2014W. http://dx.doi.org/10.1002/R016739.

Ranganathan, V., Hanor, J., 1988. Density-driven groundwater flow near salt domes. Chem. Geol. 74, 173–188.

Rao, A.M.F., McCarthy, M.J., Gardner, W.S., Jahnke, R.A., 2007. Respiration and denitrification in permeable continental shelf deposits on the South Atlantic Bight: rates of carbon and nitrogen cycling from sediment column experiments. Cont. Shelf Res. 27, 1801–1819. http://dx.doi.org/10.1016/j.csr.2007.03.001.

Reimers, C.E., Stecher, H.A., Taghon, G.L., Fuller, C.M., Huettel, M., Rusch, A., Ryckelynck, N., Wild, C., 2004. In situ measurements of advective solute transport in permeable shelf sands. Cont. Shelf Res. 24, 183–201. http://dx.doi.org/10.1016/j.csr.2003.10.005.

Rocha, C., 2000. Density-driven convection during flooding of warm, permeable intertidal sediments: the ecological importance of the convective turnover pump. J. Sea Res. 43, 1–14. http://dx.doi.org/10.1016/S1385-1101(00)00002-2.

Sanford, W.E., Whitaker, F., Smart, P., Jones, G., 1998. Numerical analysis of seawater circulation in carbonate platforms: I. Geothermal convection. Am. J. Sci. 298, 801–828.

Santos, I.R., Erler, D., Tait, D., Eyre, B.D., 2010. Breathing of a coral cay: tracing tidally driven seawater recirculation in permeable coral reef sediments. J. Geophys. Res. 115, C12010. http://dx.doi.org/10.1029/2010JC006510.

Santos, I.R., Eyre, B.D., Huettel, M., 2012. The driving forces of porewater and groundwater flow in permeable coastal sediments: a review. Estuar. Coast. Shelf Sci. 98, 1–15. http://dx.doi.org/10.1016/j.ecss.2011.10.024.

Savidge, W.B., Wilson, A.M., Woodward, G., in press. Hydrodynamic exchange in an open shelf permeable seafloor. Aquat. Geochemistry.

Sawyer, A.H., Bayani Cardenas, M., Buttles, J., 2012. Hyporheic temperature dynamics and heat exchange near channel-spanning logs. Water Resour. Res. 48, W01529. http://dx.doi.org/10.1029/2011WR011200.

Sawyer, A.H., Cardenas, M.B., 2009. Hyporheic flow and residence time distributions in heterogeneous cross-bedded sediment. Water Resour. Res. 45, W08406. http://dx.doi.org/10.1029/2008WR007632.

Schmidt, C., Büttner, O., Musolff, A., Fleckenstein, J.H., 2014. A method for automated, daily, temperature-based vertical streambed water-fluxes. Fundam. Appl. Limnol./Arch. für Hydrobiol. 184, 173–181. http://dx.doi.org/10.1127/1863-9135/2014/0548.

Smith, A.J., 2004. Mixed convection and density-dependent seawater circulation in coastal aquifers. Water Resour. Res. 40, W08309. http://dx.doi.org/10.1029/2003WR002977.

Sophocleous, M., 2002. Interactions between groundwater and surface water: the state of the science. Hydrogeol. J. 10, 52–67.

Stallman, R.W., 1963. Computation of ground-water velocity from temperature data. In: Bentall, R. (Ed.), Methods of Collecting and Interpreting Ground-Water Data. U.S. Geological Survey Water Supply Paper 1544-H, pp. 36–46.

Swanson, T.E., Cardenas, M.B., 2011. Ex-Stream: A MATLAB program for calculating fluid flux through sediment–water interfaces based on steady and transient temperature profiles. Comput. Geosci. 37, 1664–1669. http://dx.doi.org/10.1016/j.cageo.2010.12.001.

Taniguchi, M., 2000. Evaluations of the saltwater–groundwater interface from borehole temperature in a coastal region. Geophys. Res. Lett. 27, 713–716. http://dx.doi.org/10.1029/1999GL002366.

Wilson, A.M., 2003. The occurrence and chemical implications of geothermal convection of seawater in continental shelves. Geophys. Res. Lett. 30, 2127. http://dx.doi.org/10.1029/2003GL018499.

Wilson, A.M., 2005. Fresh and saline groundwater discharge to the ocean: a regional perspective. Water Resour. Res. 41. http://dx.doi.org/10.1029/2004WR003399, n/a–n/a.

Wilson, A.M., Garven, G., Boles, J.R., 1999. Paleohydrogeology of the San Joaquin basin, California. GSA Bull. 111, 432–449.

Wilson, A.M., Huettel, M., Klein, S., 2008. Grain size and depositional environment as predictors of permeability in coastal marine sands. Estuar. Coast. Shelf Sci. 80, 193–199. http://dx.doi.org/10.1016/j.ecss.2008.06.011.